International Journal of Solids and Structures 51 (2014) 1980–1990

Contents lists available at ScienceDirect

International Journal of Solids and Structures

journal homepage: www.elsevier.com/locate/ijsolstr

A method for reconstruction of residual stress fields from measurements made in an incompatible region

H.E. Coules *, D.J. Smith, K. Abburi Venkata, C.E. Truman

Department of Mechanical Engineering, University of Bristol, Bristol BS8 1TR, UK

ARTICLE INFO

Article history:
Received 29 October 2013
Received in revised form 31 January 2014
Available online 19 February 2014

Keywords:
Eigenstrain
Residual stress
Reconstruction
Finite element analysis

ABSTRACT

A method is introduced by which the complete state of residual stress in an elastic body may be inferred from a limited set of experimental measurements. Two techniques for carrying out this reconstruction using finite element analysis are compared and it is shown that for exact reconstruction of the stress field via this method, the stress field must be measured over all eigenstrain-containing regions of the object. The effects of error and incompleteness in the measured part of the stress field on the subsequent analysis are investigated in a series of numerical experiments using synthetic measurement data based on the NeT TG1 round-robin weld specimen. It is hence shown that accurate residual stress field reconstruction is possible using measurement data of a quality achievable using current experimental techniques.

1. Introduction

Residual stresses can significantly affect the mechanical performance of engineering components and structures, so for the purposes of design and structural integrity assessment it is desirable to know as much about the residual stress distribution in an object as possible (Withers, 2007; Withers et al., 2008). However, complete measurement of complex three-dimensional residual stress fields in most structural materials is currently difficult and prohibitively time-consuming (Krawitz, 2011). Consequently, most measurements are restricted to line or area scans, and fracture mechanics analyses are normally based on relatively incomplete experimental information. As a result, there is great practical value in inferring the complete residual stress field in an object from a limited number of measurements.

To date, the most successful approaches to obtaining the complete residual stress field have focussed on finding distributions of residual stress which are consistent with any measured stress/strain data and with elasticity theory. One such method is known as the inverse eigenstrain technique, and is described in detail by Jun and Korsunsky (2010). This method is based on first using the available experimental residual stress data to estimate the distribution of incompatibility, known generally as the eigenstrain tensor $\boldsymbol{\varepsilon}^*$ (Mura, 1987) in the residually-stressed body. Once the eigenstrain field has been calculated from the incomplete stress distribution (the inverse eigenstrain problem), the complete stress field can be calculated from the eigenstrain field (the 'forward' problem). To solve the inverse problem, the eigenstrain distribution must be represented using a set of basis functions. Typically, assumptions regarding the form and components of the eigenstrain distribution must be made to allow it to be represented in this way. The influence of each of these eigenstrain basis distributions on the residual stress distribution is determined using finite element analysis. The basis parameters necessary to approximate the complete eigenstrain distribution are then found by minimisation of error with respect to the experimentally-measured stress data (Korsunsky, 2009).

An alternative approach, which does not require solution of the inverse eigenstrain problem, is to approximate the residual stress distribution using a series of stress functions which automatically satisfy the equilibrium and boundary conditions (Farrahi et al., 2009). Coefficients for the series are then found such that the error between the experimental observations and the series solution is minimised (Faghidian et al., 2012; Farrahi et al., 2010).

The inverse eigenstrain and stress function approaches are most useful when the residual stress or eigenstrain distribution can be parameterised efficiently. For example, when the eigenstrain can be considered to be pointwise isotropic, or to vary in only one dimension (Achintha et al., 2013; DeWald and Hill, 2006; Korsunsky and Regino, 2007). However these approaches are more difficult to apply for a general three-dimensional stress distribution, since the number of basis functions required rapidly becomes large. Furthermore, some *a priori* knowledge of the eigenstrain distribution is often required so that basis functions can be chosen which minimise the required number of experimental data. Both of

* Corresponding author. Tel.: +44 (0)117 331 5941.
E-mail address: harry.coules@bristol.ac.uk (H.E. Coules).

http://dx.doi.org/10.1016/j.ijsolstr.2014.02.008
0020-7683/

these issues are of practical significance, because residual stress analysis must often be carried out on complex engineering components containing states of residual stress which cannot be simply represented.

In this work, we propose an alternative method of residual stress field reconstruction which can be used when incompatibility is localised to some portion $\mathcal{B}_1$ of the object (Fig. 1a). In this case the complete stress field can be reconstructed from measurements taken in the incompatible region without determination of the eigenstrain distribution, thus making measurement of residual stresses in the rest of the object (i.e. region $\mathcal{B}_2$) unnecessary. This method is implemented using Finite Element (FE) analysis, and a numerical study is presented here in which the residual stresses in a benchmark weld specimen, shown in Fig. 2, are reconstructed. It is shown that the new method enables measurement strategies that focus on the incompatible region of interest rather than measuring residual elastic strains everywhere. The principles of the method are described, followed by the implementation in finite element analysis using two approaches. The method is then applied to the benchmark weld specimen shown in Fig. 2, and the results are discussed with reference to the inverse eigenstrain and stress function methods.

2. Principles of the proposed method

A residual stress field in a solid body is not uniquely defined by the object's geometry, material properties and boundary conditions as is the case for stress fields which arise solely from external loading (Timoshenko and Goodier, 1970). Instead, residual stresses also depend on the internal incompatibility within the body. The distribution of incompatible strain in such a body is known as the eigenstrain distribution, and the total strain ($\boldsymbol{\varepsilon}$) is expressed as the sum of elastic ($\boldsymbol{e}$) and eigenstrain ($\boldsymbol{\varepsilon}^*$) terms (Mura, 1987):

$$\boldsymbol{\varepsilon} = \boldsymbol{e} + \boldsymbol{\varepsilon}^* \tag{1}$$

For a continuous distribution of deformations to occur, the total strain must be compatible. Hence, the small-strain compatibility equations for a three-dimensional body in the presence of eigenstrain are (Mura, 1987; Korsunsky, 2009):

$$\begin{aligned}
&\frac{\partial^2 e_{xx}}{\partial y^2}+\frac{\partial^2 e_{yy}}{\partial x^2}-2\frac{\partial^2 e_{xy}}{\partial x\partial y}=\Xi_1=-\frac{\partial^2 \varepsilon^*_{xx}}{\partial y^2}-\frac{\partial^2 \varepsilon^*_{yy}}{\partial x^2}+2\frac{\partial^2 \varepsilon^*_{xy}}{\partial x\partial y}\\
&\frac{\partial^2 e_{yy}}{\partial z^2}+\frac{\partial^2 e_{zz}}{\partial y^2}-2\frac{\partial^2 e_{yz}}{\partial y\partial z}=\Xi_2=-\frac{\partial^2 \varepsilon^*_{yy}}{\partial z^2}-\frac{\partial^2 \varepsilon^*_{zz}}{\partial y^2}+2\frac{\partial^2 \varepsilon^*_{yz}}{\partial y\partial z}\\
&\frac{\partial^2 e_{zz}}{\partial x^2}+\frac{\partial^2 e_{xx}}{\partial z^2}-2\frac{\partial^2 e_{zx}}{\partial z\partial x}=\Xi_3=-\frac{\partial^2 \varepsilon^*_{zz}}{\partial x^2}-\frac{\partial^2 \varepsilon^*_{xx}}{\partial z^2}+2\frac{\partial^2 \varepsilon^*_{zx}}{\partial z\partial x}\\
&\frac{\partial^2 e_{xx}}{\partial y\partial z}+\frac{\partial}{\partial x}\left(-\frac{\partial e_{yz}}{\partial x}+\frac{\partial e_{zx}}{\partial y}+\frac{\partial e_{xy}}{\partial z}\right)=\Xi_4=-\frac{\partial^2 \varepsilon^*_{xx}}{\partial y\partial z}-\frac{\partial}{\partial x}\left(-\frac{\partial \varepsilon^*_{yz}}{\partial x}+\frac{\partial \varepsilon^*_{zx}}{\partial y}+\frac{\partial \varepsilon^*_{xy}}{\partial z}\right)\\
&\frac{\partial^2 e_{yy}}{\partial z\partial x}+\frac{\partial}{\partial y}\left(\frac{\partial e_{yz}}{\partial x}-\frac{\partial e_{zx}}{\partial y}+\frac{\partial e_{xy}}{\partial z}\right)=\Xi_5=-\frac{\partial^2 \varepsilon^*_{yy}}{\partial z\partial x}-\frac{\partial}{\partial y}\left(\frac{\partial \varepsilon^*_{yz}}{\partial x}-\frac{\partial \varepsilon^*_{zx}}{\partial y}+\frac{\partial \varepsilon^*_{xy}}{\partial z}\right)\\
&\frac{\partial^2 e_{zz}}{\partial x\partial y}+\frac{\partial}{\partial z}\left(\frac{\partial e_{yz}}{\partial x}+\frac{\partial e_{zx}}{\partial y}-\frac{\partial e_{xy}}{\partial z}\right)=\Xi_6=-\frac{\partial^2 \varepsilon^*_{zz}}{\partial x\partial y}-\frac{\partial}{\partial z}\left(\frac{\partial \varepsilon^*_{yz}}{\partial x}+\frac{\partial \varepsilon^*_{zx}}{\partial y}-\frac{\partial \varepsilon^*_{xy}}{\partial z}\right)
\end{aligned} \tag{2}$$

where $\boldsymbol{\Xi}(x,y,z) = [\,\Xi_1 \ \ldots \ \Xi_6\,]^T$ is the forcing term which results from the incompatibility in eigenstrain on the right hand side of the equations. In a fully compatible body (i.e. $\boldsymbol{\varepsilon}^* = 0$), the forcing term $\boldsymbol{\Xi}$ is equal to zero throughout. Any distribution of eigenstrain which produces finite forcing terms causes a finite and incompatible distribution of elastic strain.

Finding the distribution of residual stress which results from a known eigenstrain field is known as the 'forward' or 'direct' problem of eigenstrain. The stress distribution is found by solving the compatibility equations simultaneously with the equations of stress equilibrium and any boundary conditions (Korsunsky, 2009). For a body containing only residual stresses, the boundary conditions are that the body must be traction-free at all boundaries. In the absence of body forces, equilibrium is described by:

$$div\,\boldsymbol{\sigma} = 0 \tag{3}$$

where $\boldsymbol{\sigma}$ is the stress tensor, which for a linearly-elastic material is related via Hooke's law to the elastic strain:

$$\boldsymbol{\sigma} = \boldsymbol{C} : \boldsymbol{e} \tag{4}$$

where $\boldsymbol{C}$ is the stiffness tensor. Therefore, if the eigenstrain distribution and elastic properties of a solid body are known, the residual stress distribution can be calculated. Solution of the forward eigenstrain problem in this way has widespread application in engineering and micromechanics (Mura, 1987), and is the subject of several classic papers including Eshelby's well-known solution for the case of an ellipsoidal inclusion (Eshelby, 1957).

Combining the compatibility equations (Eq. (2)) with Hooke's law (Eq. (4)) allows the forcing term $\boldsymbol{\Xi}$ to be found from a known stress field. For example, for an isotropic and linearly elastic material the first compatibility equation yields:

$$\Xi_1 = \frac{1}{E}\left[\frac{\partial^2}{\partial y^2}(\sigma_{xx} - \nu(\sigma_{yy}+\sigma_{zz})) + \frac{\partial^2}{\partial x^2}(\sigma_{yy} - \nu(\sigma_{zz}+\sigma_{xx})) - 2(1-\nu)\frac{\partial^2 \tau_{xy}}{\partial x\partial y}\right] \tag{5}$$

where E is the material's elastic modulus, and ν is Poisson's ratio. For a body $\mathcal{B}$ which contains finite eigenstrain over only part of its volume (Fig. 1a), knowledge of the stress field in the eigenstrain-containing (i.e. incompatible) region $\mathcal{B}_1$ is sufficient to characterise the forcing term $\boldsymbol{\Xi}(\mathbf{x})$, $\mathbf{x} \in \mathcal{B}_1$. In region $\mathcal{B}_2$ there is no eigenstrain, so: $\boldsymbol{\Xi}(\mathbf{x}) \equiv 0$, $\mathbf{x} \in \mathcal{B}_2$. With the forcing term known for the whole body, it is possible to calculate the complete residual stress field.

3. Implementation

3.1. Finite element implementation

Eq. (5) suggests that if the stress field in the incompatible region $\mathcal{B}_1$ is known, it can be used (in lieu of the eigenstrain distribution) to infer the stress field in the rest of the body: stresses elsewhere in the body $\mathcal{B}$ can be inferred by imposing the known/measured stress distribution over $\mathcal{B}_1$ and finding the compatible distribution of elastic strain in $\mathcal{B}_2$ that is in equilibrium with it. Two methods of inferring the complete stress field from using finite element analysis are used in this study (Fig. 3). These are referred to as the 'direct' and 'iterative' methods.

In the direct method, $\mathcal{B}_1$ is considered alone (see Fig. 1b) and zero-displacement conditions are imposed at the interface $\partial(\mathcal{B}_1/\mathcal{B}_2)$. The nodal forces which represent the tractions on this interface are then found from the stress distribution. Finally, by considering $\mathcal{B}_2$ alone and applying the tractions found in the previous step to the $\partial(\mathcal{B}_1/\mathcal{B}_2)$ interface, the stress distribution in region $\mathcal{B}_2$ is calculated from the resulting boundary-value problem.

The second technique is an iterative method. The FE solver used in this study includes a procedure by which local equilibrium of the stress field can established after a predefined stress field which does not satisfy equilibrium has been imposed (Abaqus Analysis User's Manual v6.12, 2012). In this method, an equal and opposite stress state is applied to the whole body resulting in zero stress throughout. This opposite stress state is then gradually reduced, and the resulting (self-equilibrating) stress field is calculated elastically. This process allows the predefined part of the stress field to change, so it is necessary to run the process iteratively: taking the stress distribution for the whole body from the previous iteration, re-applying the known stresses in $\mathcal{B}_1$, and finding the new

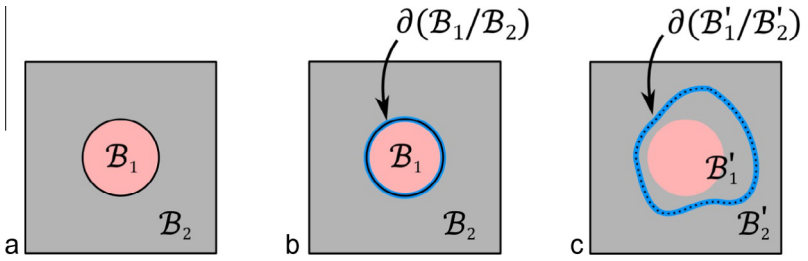

Fig. 1. (a) Residually-stressed body $\mathcal{B}$ with eigenstrain-containing region $\mathcal{B}_1$ and compatible region $\mathcal{B}_2$. (b) The boundary $\partial(\mathcal{B}_1/\mathcal{B}_2)$ separates regions $\mathcal{B}_1$ and $\mathcal{B}_2$. (c) The boundary $\partial(\mathcal{B}'_1/\mathcal{B}'_2)$, where $\mathcal{B}_1 \in \mathcal{B}'_1$.

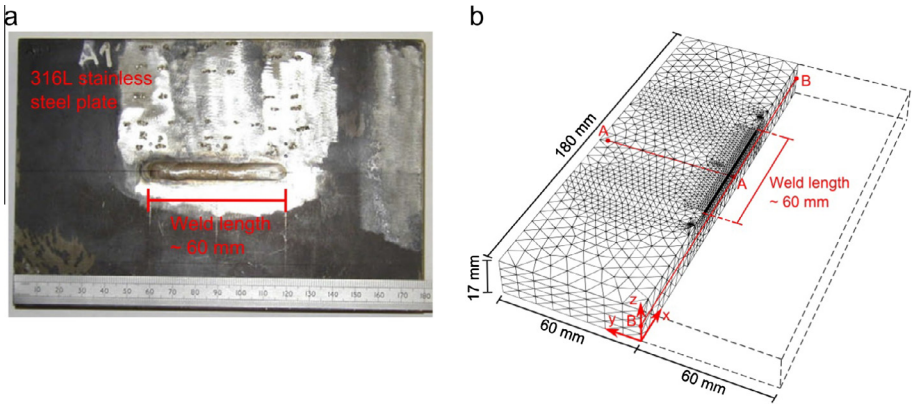

Fig. 2. The Net TG1 benchmark weld specimen: (a) photograph of the TG1 specimen A11 (Bouchard, 2009), (b) weld geometry, showing the finite element mesh used for all models described in this paper. The A–A and B–B lines, both of which lie at the mid-thickness of the plate ($z = 8.5$ mm), are referred to in the results. Fig. 2a reprinted from Bouchard, 2009 with permission from Elsevier.

equilibrium state. This is illustrated in Fig. 3. The stress field gradually converges to a solution which satisfies the equilibrium equations, while having the correct known stress distribution in region $\mathcal{B}_1$. This method has been previously been used in other studies to infer longer-range residual stresses from deep-hole drilling measurements (Do et al., 2013; Ficquet, 2007).

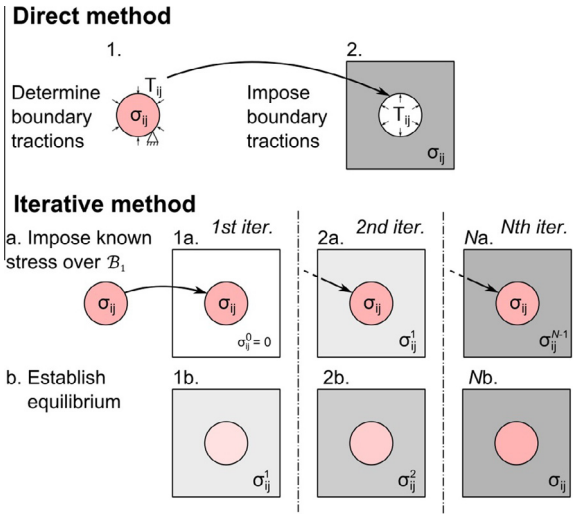

Fig. 3. Two schemes for finding the complete residual stress field from stresses in the incompatible region $\mathcal{B}_1$. The direct method uses the tractions at the $\mathcal{B}_1$ boundary, which are imposed on a model of the rest of the object. In the iterative method, the $\mathcal{B}_1$ stress field is repeatedly imposed on a model of the complete object.

3.2. Measurement considerations

The reconstruction methods described above are applicable when material incompatibility is limited to some region $\mathcal{B}_1$ of an object. To apply such methods, it is necessary to measure or assume the dimensions of this incompatible region. Since incompatibility results from inelastic deformation, the size of the incompatible region can be estimated from measurements of material plasticity. In most metals, plastic deformation results in strain-hardening and so large-scale plasticity can often be identified using hardness measurements (Bouras et al., 2012). Also, it is often possible to quantify (or at least identify) prior plastic deformation in metals using synchrotron or neutron diffraction data via analysis of diffraction peak broadening or anisotropy of the lattice strain response (Daymond et al., 1997; Hutchings, 1992). This method has previously been used to define the eigenstrain-containing region for inverse eigenstrain analysis (Achintha et al., 2013; Jun et al., 2012). If the size of the eigenstrain-containing region is overestimated, as illustrated in Fig. 1c, and measurements are obtained from the larger region $\mathcal{B}'_1$ where $\mathcal{B}_1 \in \mathcal{B}'_1$, this will cause no error in the stress field calculated for $\mathcal{B}'_2$. In the part of $\mathcal{B}'_1$ which is compatible, the forcing terms in Eq. (2) will be equal to zero and therefore will have no effect on the reconstructed stress distribution. If, on the other hand, the size of the incompatible region is underestimated and residual stress measurements are only taken over a smaller region, part of the eigenstrain distribution is omitted. This causes errors in the reconstructed stress field (see Ficquet, 2007; Lei et al., 2000).

For a complete definition of the residual stress field inside region $\mathcal{B}_1$, all independent components of the stress tensor would have to be measured. However, most methods of residual elastic strain measurement cannot determine all (six) components in the general

three-dimensional case. In principal, neutron and synchrotron X-ray diffraction are capable of measuring all six components. However, even with these methods it is uncommon to attempt to measure shear stresses (Krawitz, 2011). This makes it necessary either to assume that the measured directions are principal, or accept that unknown shear stresses may be present (Winholtz and Krawitz, 1996). Finally, practical residual stress measurements have finite spatial resolution, so the representation of the stress distribution in $\mathcal{B}_1$ from measured data would be discretised. The effects of these measurement limitations on the accuracy of the reconstructed stress fields are investigated later in this article.

4. Numerical example

In this section, results from a finite element simulation of the welding of a benchmark weld specimen (shown in Fig. 2) are used to explore the application of the methods of stress field reconstruction outlined above. It is first shown that the two methods (direct and iterative) are able to reconstruct the weld residual stress field when provided with 'ideal' input data. Later, a series of parametric experiments are used to investigate the suitability of these methods when applied to practical experimental data.

4.1. Target residual stress field

The residual stress field shown in Fig. 4 is the result of a finite element model of the benchmark weld specimen illustrated in Fig. 2. The weld was a single-pass bead-on-plate TIG weld in AISI type 316L austenitic stainless steel known as the NeT TG1 specimen. This was used in a previous round-robin study involving both residual stress measurements and weld models (Bouchard, 2009; Smith and Smith, 2009). The overall dimensions of the specimen are $180 \times 120 \times 17$ mm^3 with a nominal weld length of 60 mm (see Fig. 2a). The geometry and process parameters of the NeT TG1 specimen were used in a sequentially-coupled thermo-mechanical finite element analysis of the welding process, which generated a target residual stress state for use in testing stress reconstruction methods. The weld analysis was carried out using Abaqus/Standard 6.12, with transient heat flux implemented via the DFLUX user subroutine. In order to reduce the computation time only half of the specimen was modelled, with symmetric boundary conditions applied at the centre of the weld. The mesh consisted of 94,092 nodes and 66,728 ten-node quadratic tetrahedral elements (Abaqus type C3D10), with the mesh density weighted heavily towards the weld region, as shown in Fig. 2. In this initial process model, all material properties were considered to be temperature-dependent. The resulting residual stress distribution shown in Fig. 4 is typical for a weld of this type, and agrees closely with experimental and modelled results for the TG1 specimen presented during the NeT round-robin study (Smith and Smith, 2009).

The results of the weld model (shown in Fig. 4) provide a target "true" residual stress state for assessing the stress field reconstruction procedures. The target distribution is well-characterised, and this permits direct comparison between the target and reconstructed stress fields. To avoid interpolation of the target stress field, the same FE mesh geometry was used in both the initial weld model and all of the subsequent models used to reconstruct the stress state. The materials' ambient-temperature elastic properties, required for the reconstruction procedures, were the same as those used in the weld model.

4.2. Reconstruction details

The direct and iterative reconstruction methods were implemented using a fully-elastic FE model of the NeT TG1 specimen created using the same geometry and mechanical boundary conditions as the initial weld model. The implicit solver used for all FE calculations required for the reconstruction procedures was Abaqus/Standard 6.12 (Abaqus Analysis User's Manual v6.12, 2012). Routines written in MATLAB code (MATLAB, 2012) were used to automatically write the solver input files necessary for the large number of iterative analyses, to read and post-process the results, and to link the different parts of each analysis method.

For the iterative method each individual analysis procedure, representing a single iteration, consisted of two steps shown in Fig. 3: an initial step in which the known stress components in the 'measurement' region were applied, followed by an equilibrium step in which the stress field was allowed to equilibrate throughout the object. For each iteration, a solver input file was written. This contained the initial stress field data for the iteration: any known stresses in the 'measurement' region, plus the remainder of the stress field taken from the previous iteration. After the iteration had run, the stress field data was automatically extracted from the output files for use in the next iteration.

The direct method used a different two-step analysis procedure. In the first step, all elements except those in the 'measurement' region were de-activated, and additional boundary conditions were added such that the newly-exposed edges of this region were prevented from moving. The known stress field in the 'measurement' region was imposed at the start of the analysis step, and the resulting forces on the fixed interface nodes were found. In the second step, the measurement region (rather than the surrounding region) was deactivated and the nodal forces found from the first step were imposed at the interface nodes. This allowed the resulting stress field in the remaining (compatible) part of the object to be calculated.

4.3. Reconstruction using ideal 'measurement' data

In addition to the residual stress field, the initial weld model provided information about plastic deformation created during the weld simulation. At the start of the weld model the material was taken to be completely compatible and to contain no residual stress. Therefore, after welding the eigenstrain tensor was only non-zero in regions that had undergone plastic deformation during welding. It follows that the region of plastic deformation in the weld model encompasses any eigenstrain-containing regions, and will therefore be sufficient for calculating the remainder of the stress field. The calculated von Mises equivalent plastic strain created in the weld model is shown in Fig. 5a, and the residual stress field (σ_{xx} component) for the part of the object which undergoes a finite plastic strain during welding is shown in Fig. 5b. This plastic region accounts for approximately 17% of the total volume of the welded plate.

Reconstructions via the direct and iterative methods were carried out using all components of the 'measured' stress tensor from the plastic region; Fig. 6 shows the resulting complete stress fields. The stress fields reconstructed using both the iterative (Fig. 6a–c) and direct (Fig. 6d–f) methods are practically identical to the target field (Fig. 4).

To compare the target and reconstructed residual stress fields, the total elastic strain energy of each of the two fields was evaluated. Although total elastic strain energy is a scalar and cannot uniquely describe the whole stress distribution, it is useful for comparing similar stress fields. Fig. 7a shows convergence of the iterative method towards the target stress distribution (Fig. 4) in terms of the total strain energy. The total strain energy of the iteratively-reconstructed field rapidly approaches that of the target field (5.82 J). However, even after 100 iterations the difference in total strain energy (5.73 J) indicates that there remain minor differences in the reconstructed distribution, which can be attributed to discretisation and numerical errors. The maximum longitudinal

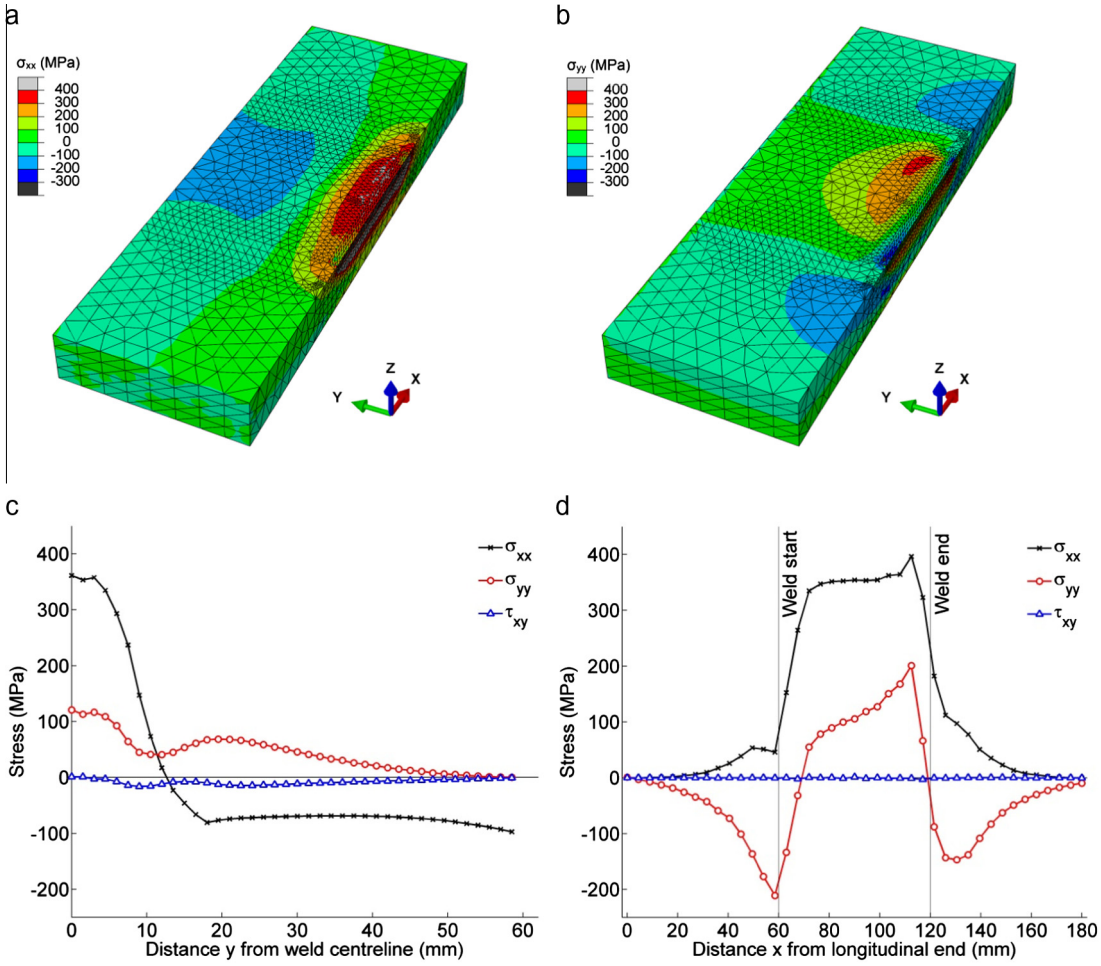

Fig. 4. Target residual stress distribution generated by a weld simulation of the NET TG1 specimen: (a) longitudinal component (σ_{xx}), (b) transverse component (σ_{yy}), (c) in-plane stress components along the A–A line (see Fig. 2b), (d) in-plane stress components along the B–B line.

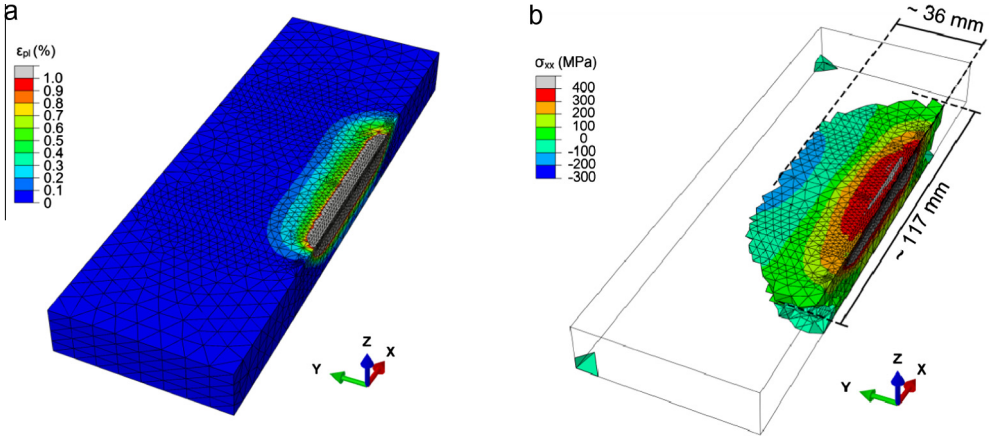

Fig. 5. (a) Plastic deformation (von Mises equivalent) during welding in NeT TG1 specimen (modelled), (b) longitudinal (σ_{xx}) residual stress distribution in the region of finite plastic strain ($\varepsilon_{pl} > 1$ με).

tensile stress at any point in the field is shown in Fig. 7b, and also shows good convergence.

5. Parametric studies using non-ideal 'measurement' data

As discussed in Section 3.2, experimental measurements of residual stress are generally limited in spatial resolution, in strain resolution, and in terms of the number of stress/strain tensor components measured. Furthermore, the eigenstrain distribution is not generally known *a priori*. The effect of these factors on the accuracy of the reconstructed stress field was studied using four parametric series of reconstructions. First the size of the measurement region was studied, followed by the available components of the stress tensor, finite spatial resolution, and the effects of random errors in strain measurement. Finally, all of these factors were used

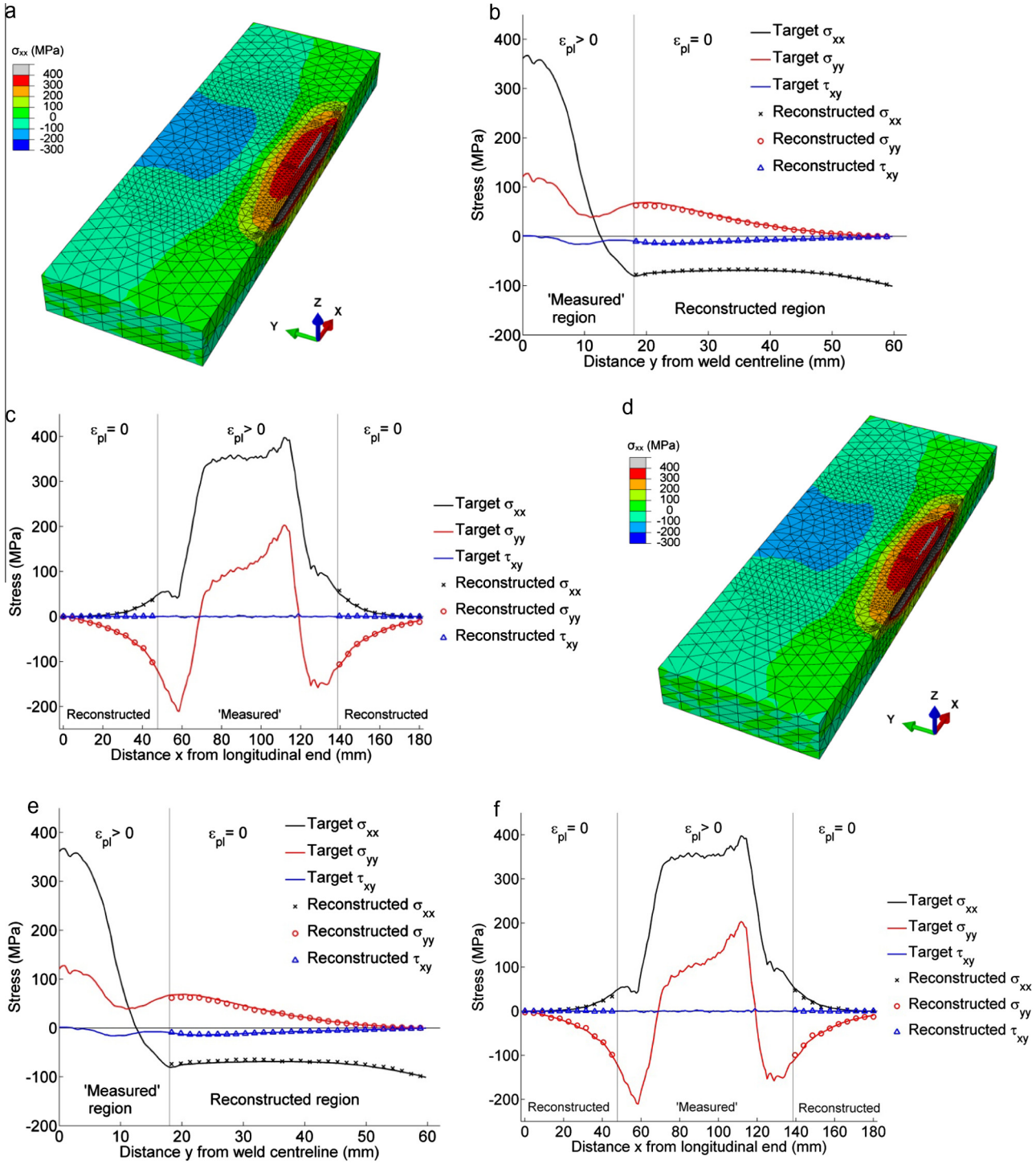

Fig. 6. Reconstruction of the complete stress field from the portion shown in Fig. 5b. (a–c) Reconstruction via the iterative method (100 iterations). (d–f) Reconstruction via the direct method. Sub-plots (b) and (e) show line plots along the A–A line. Sub-plots (c) and (f) show the B–B line (see Fig. 2b).

simultaneously to create a feasible data set of synthetic measurement data, and a reconstruction was carried out using this to examine their combined effect.

5.1. Size of measurement region

Reconstruction of the complete residual stress field was carried out using data from 'measurement' regions of decreasing volume. In the previous section, the stress field was reproduced almost perfectly from data covering the whole of the region which undergoes plasticity during the initial weld model. Smaller measurement regions were defined by taking the region of the weld which had undergone increasing values of equivalent plastic strain. Thirteen such synthetic 'measurement' regions were defined using plastic strain limits logarithmically spaced between 1 and 10^4 με. Reconstructed stress fields are shown in Fig. 8, with longitudinal stresses (σ_{xx}) shown for three levels of plastic strain: 215, 1000 and 2154 με. The errors between the reconstructed and target stress fields (in terms of the total strain energy) for all thirteen measurement region sizes are shown in Fig. 9. Greater errors occur as larger

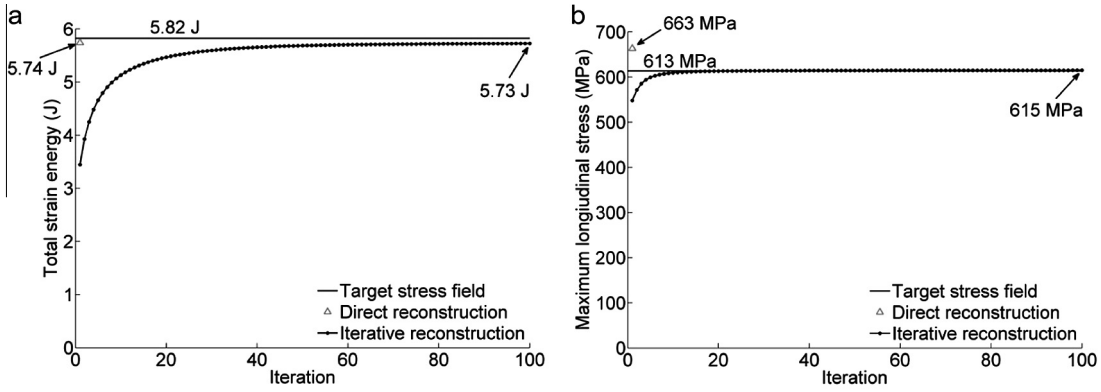

Fig. 7. Reconstruction using ideal 'measurement' data. Convergence of: (a) total elastic strain energy, (b) maximum tensile stress in the longitudinal direction.

plastic strain limits defining the 'measurement' region are used (i.e. as the region is reduced in size). The divergence from the target stress state is more rapid for the direct method than for the iterative.

5.2. Available stress tensor components

A second parametric trial was used to investigate the effect on the reconstructed stress field when only certain components of the stress tensor are available in the 'measurement' data. Using the same measurement region as shown in Fig. 5b, reconstructions were attempted using:

- All six components of the stress tensor.
- The three normal components σ_{xx}, σ_{yy} and σ_{zz} and the in-plane shear τ_{xy}.
- The three normal components σ_{xx}, σ_{yy} and σ_{zz} only.
- Only the σ_{xx} and σ_{yy} components.
- Only the σ_{xx} component.

For reconstruction using a limited set of stress tensor components via the iterative method, all of the tensor components were mapped from the result of each iteration to the initial state of the subsequent one. However, only the components specified above were then forced back to their 'measured' values in the measurement region. For brevity, only the errors between the target and reconstructed total elastic strain energy will be discussed for the remaining parametric studies; these are shown in Fig. 10. As shown in Fig. 10a, when only the σ_{xx} component or only the σ_{xx} and σ_{yy} components are used, neither the direct nor the iterative method is able to reproduce the target distribution accurately, leading to errors of >15% in the total strain energy. However, when provided with all three of the normal components in the 'measurement' region it is possible to reproduce the target stress distribution accurately via the iterative method. The shear components of the residual stress distribution throughout the object are reconstructed accurately, despite there being no information about the shear stress given in the reconstruction's input data. The spatial variation in the three provided components of the stress tensor is sufficient to calculate the other three components in the measurement region, and consequently the remainder the stress field can also be inferred with reasonable accuracy.

5.3. Finite spatial resolution

In this set of reconstructions, the same 'measurement' region (Fig. 5b) was used, as were all components of the stress tensor in this region. To simulate the effect of a finite measurement resolution, the 'measurement' data were spatially averaged over approximately cubic volumes (the sizes of which are given in Table 1) before being used in the reconstruction procedure. The volumes are aligned with the specimen coordinate axes and are not intended to represent diffraction scattering volumes, but rather to simulate the fine spatial resolution of an arbitrary strain measurement method.

Although the 'measurement' data were spatially averaged, it is important to note that the FE mesh was not modified: as in all previous reconstructions the averaged data was simply applied element-wise at the element integration points, preventing any numerical effects of mesh coarsening from influencing the result. The errors between the reconstructed and target strain energies are shown in Fig. 10b. For both the direct and iterative reconstruction methods the accuracy of the reconstructed stress state decreases considerably when the spatial averaging resolution exceeds a volume of $5 \times 5 \times 5$ mm.

5.4. Random errors

In this final set of parametric reconstructions, normally-distributed random errors in residual strain determination were simulated, and propagated through the Hooke's law calculation of stress in the measurement region (using the relations given by Wimpory et al. (2009a,b)). Reconstruction of the complete stress field was then carried out using this error-containing stress data. The results (Fig. 10c) show that errors in strain determination with a standard deviation of >100 με can cause the error in the total strain energy of the reconstructed field to exceed 5%.

5.5. Combined effect

In addition to the parametric studies described above, one reconstruction was carried out to study the combined effect of several types of incompleteness and error in the initial data. The synthetic measurement data were designed to mimic current neutron or synchrotron diffraction capabilities. This synthetic residual stress data had a limited spatial resolution of approximately $2.5 \times 2.5 \times 2.5$ mm (grid no. 5, given in Table 1), contained only σ_{xx}, σ_{yy}, σ_{zz}, and τ_{xy} stress components, and was limited to regions which had undergone $\geqslant 1000$ με equivalent plastic strain during welding. Normally-distributed random errors in strain measurement with a standard deviation of 50 με were also included, and reconstruction was carried out using the iterative method with 100 iterations.

Fig. 11 shows the results of the reconstruction. Irrespective of the incompleteness, discretisation and noise in the synthetic measurement data, the reconstructed part of the stress field shows good agreement with the original target field (Fig. 4), with the greatest inaccuracies occurring in the transition from the measurement region to the reconstructed region.

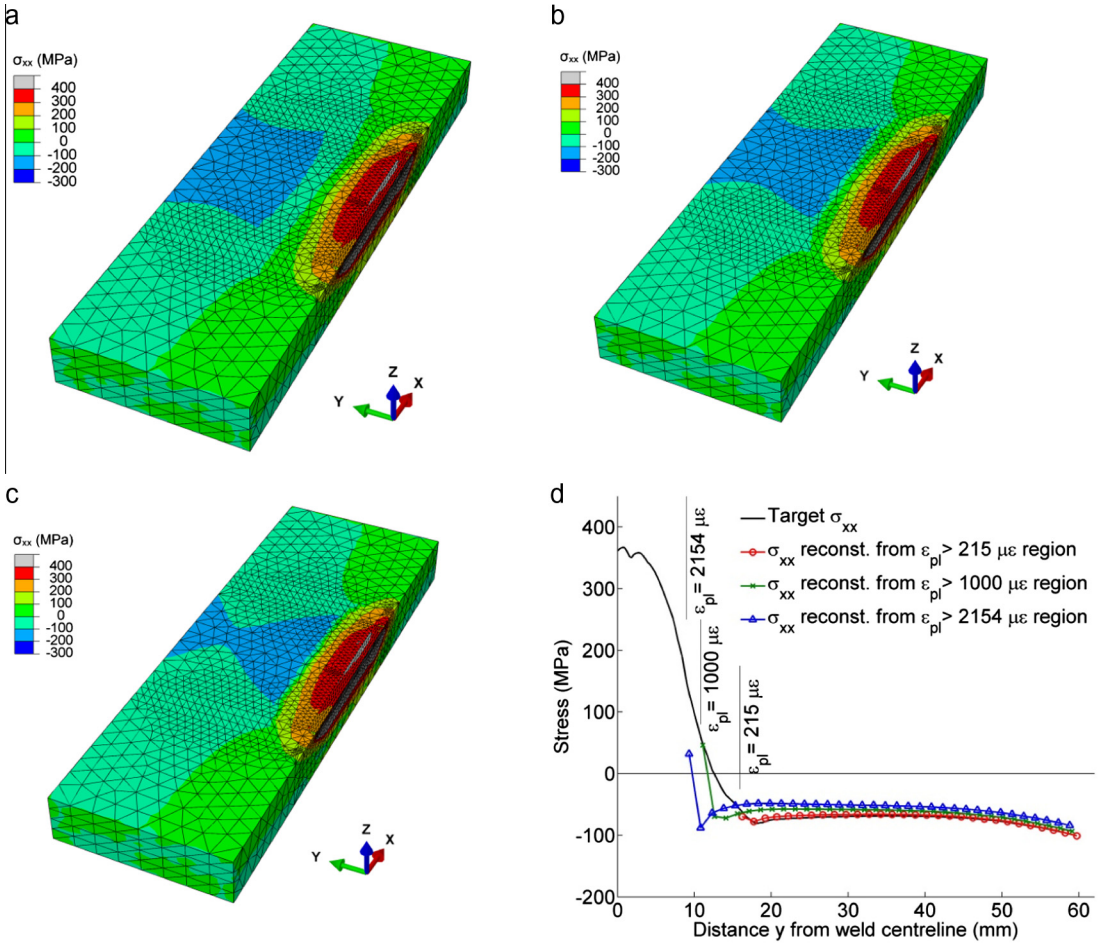

Fig. 8. Imperfect reconstruction of the stress field occurs when stress 'measurements' are not provided for the whole eigenstrain-containing region. For the iterative method (100 iterations), plastic strain limits of: (a) 215 με, (b) 1000 με, (c) 2154 με give total elastic strain energy errors of 1.51%, 3.59% and 8.13%, respectively. (d) Shows the σ_{xx} component along the A–A line (see Fig. 2b).

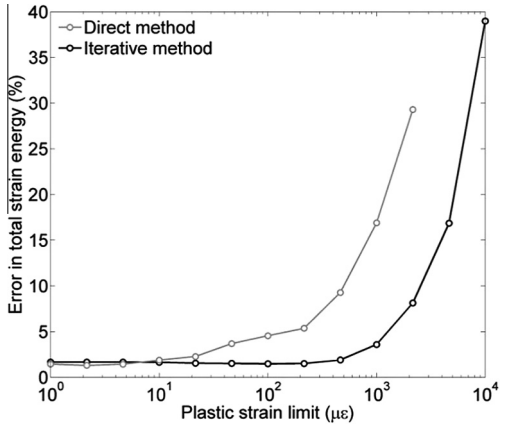

Fig. 9. Error in the total strain energy of the reconstructed field resulting from a reduced measurement region size (defined by limits of equivalent plastic strain undergone during welding).

6. Discussion

6.1. Applicability to experimental measurements

The reconstructions using ideal 'measurement' data confirm that when the stress field inside the incompatible region of a residually-stressed body is known (along with any mechanical boundary conditions and elastic properties) the residual stress field throughout the rest of the body can be calculated. Most current experimental methods could not provide such a complete characterisation of the stress state in the incompatible region. However, the parametric studies in Section 5 demonstrate that even with an incomplete and error-prone synthetic measurement of the incompatible region, the remainder of the stress distribution can be inferred with good accuracy.

The spatial resolution and number of strain tensor components used in the study of the combined effects (Section 5.5) can be obtained using current experimental methods. A resolution of around 2.5 mm is readily achieved using diffraction-based techniques (Withers and Bhadeshia, 2001). For reconstruction of a three-dimensional stress field it is necessary to first obtain a three-dimensional map of part of it. However, current diffraction measurements of residual elastic strain are restricted (largely by time constraints) to line and area scans. Nevertheless, in recent years improved instrumentation and new experimental techniques (such as the spiral slit technique in synchrotron X-ray diffraction (Martins et al., 2010) suggest that such three-dimensional measurements are feasible, making it possible to apply the reconstruction techniques described here to three-dimensional residual stress fields.

Defining the extent of the measurement region required to accurately infer the remaining residual stress field is more difficult. The reconstruction results for the NeT TG1 specimen confirm that reconstruction is possible if the measurement region includes all

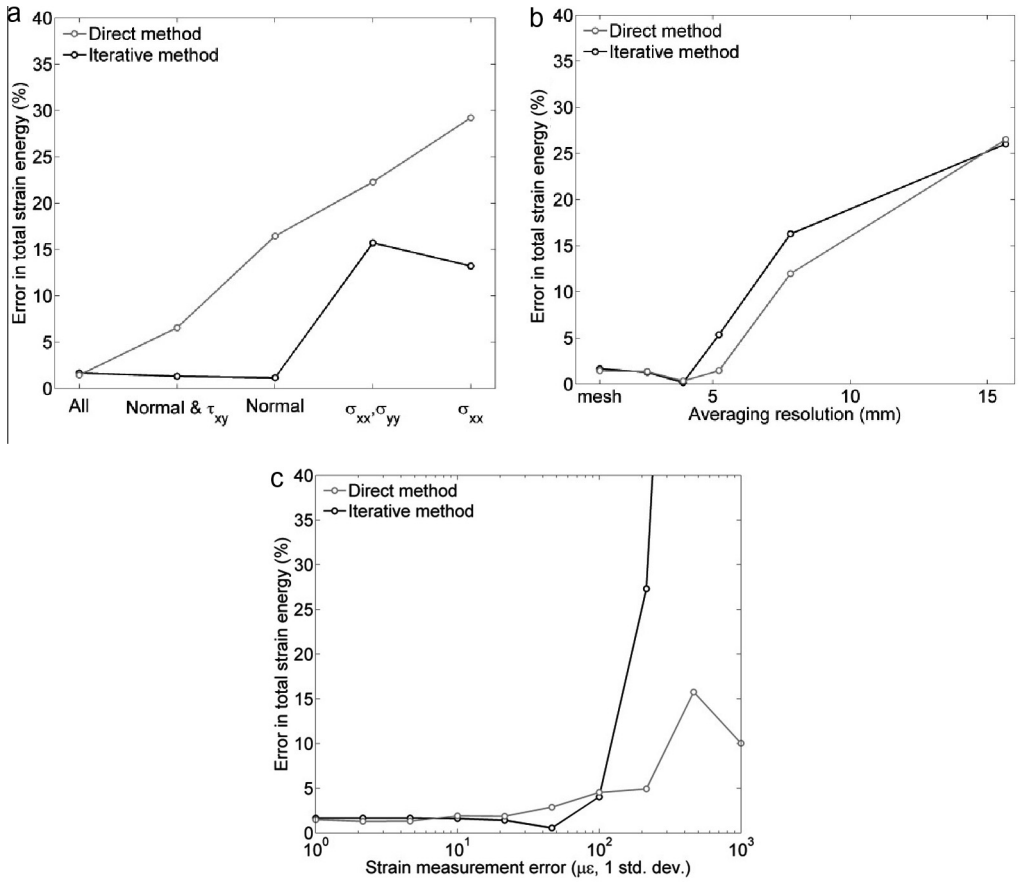

Fig. 10. Errors in the reconstructed field due to: (a) the use of only certain 'measured' stress tensor components, (b) spatial averaging of the simulated measurement data, (c) normally-distributed random errors in the simulated measurements. All iterative method results are for 100 iterations.

Table 1
Averaging volumes used to study the effect of measurement spatial resolution on reconstruction of the complete residual stress field. Note the averaging resolutions in z are integer fractions of thickness of the NeT TG1 specimen (17 mm).

Grid no.	Resolution (mm)				Averaging volume (mm^3)
	x	y	z	mean	
1	15	15	17	15.7	3825
2	7.5	7.5	8.5	7.83	478
3	5	5	5.67	5.22	142
4	3.75	3.75	4.25	3.92	59.8
5	2.5	2.5	2.83	2.61	17.7

locations that contain a finite eigenstrain (see Section 4.3). Furthermore, it was possible to reconstruct the stress field to reasonable accuracy even when a significant fraction of the plastic zone (i.e. a significant fraction of the eigenstrain-containing region) was excluded from the 'measurement' data. In collecting residual stress data suitable for the use with this new technique, it would be necessary to ensure that the majority of the eigenstrain-containing region(s) was measured: either using some *a priori* knowledge or assumption regarding its extent, or by inferring it from measurements of related variables, such as hardness or dislocation density.

6.2. Comparison of the direct and iterative methods

The direct and iterative methods both give equivalently accurate reconstructions of the residual stress state when ideal 'measurement' data are provided. In terms of computation time, the direct method is significantly faster: including all pre- and post-processing, each of the direct method reconstructions shown here took approximately 21 min on a PC with a 3.10 GHz Intel Core i7 CPU and 8 GB of memory, compared with 690 min for 100 iterations using the iterative method. However, it can be seen from Figs. 9 and 10 that when non-ideal data are used, the results for the different reconstruction processes diverge. The direct method is significantly more sensitive than the iterative method to a reduced measurement region (Fig. 9). This was also the case in the use of only three or four measured stress tensor components rather than six (Fig. 10a). However the direct method was slightly less error-prone than the iterative method when provided with spatially-averaged data (Fig. 10b). These differences are associated with the FE implementation of the direct technique used here: for the first step of the direct method, in which the measurement region's boundary tractions are determined (see Section 3), it is necessary to ensure that all elements in the region onto which the 'measurement' stresses are mapped have a sufficient number of connected nodes. This was done by adding an initially stress-free interface layer containing all elements outside of the measurement region that contact the boundary. The presence of this layer causes small errors in the calculated boundary tractions, which can cause additional errors in the reconstructed field when used with an incomplete eigenstrain distribution. Therefore, because the iterative method has a greater tolerance to incomplete characterisation of the stress field in the incompatible region, it is recommended in preference to the direct method.

6.3. Comparison with inverse eigenstrain and stress function methods

The inverse eigenstrain method, stress function-based methods, and the method presented here all work on the principle of

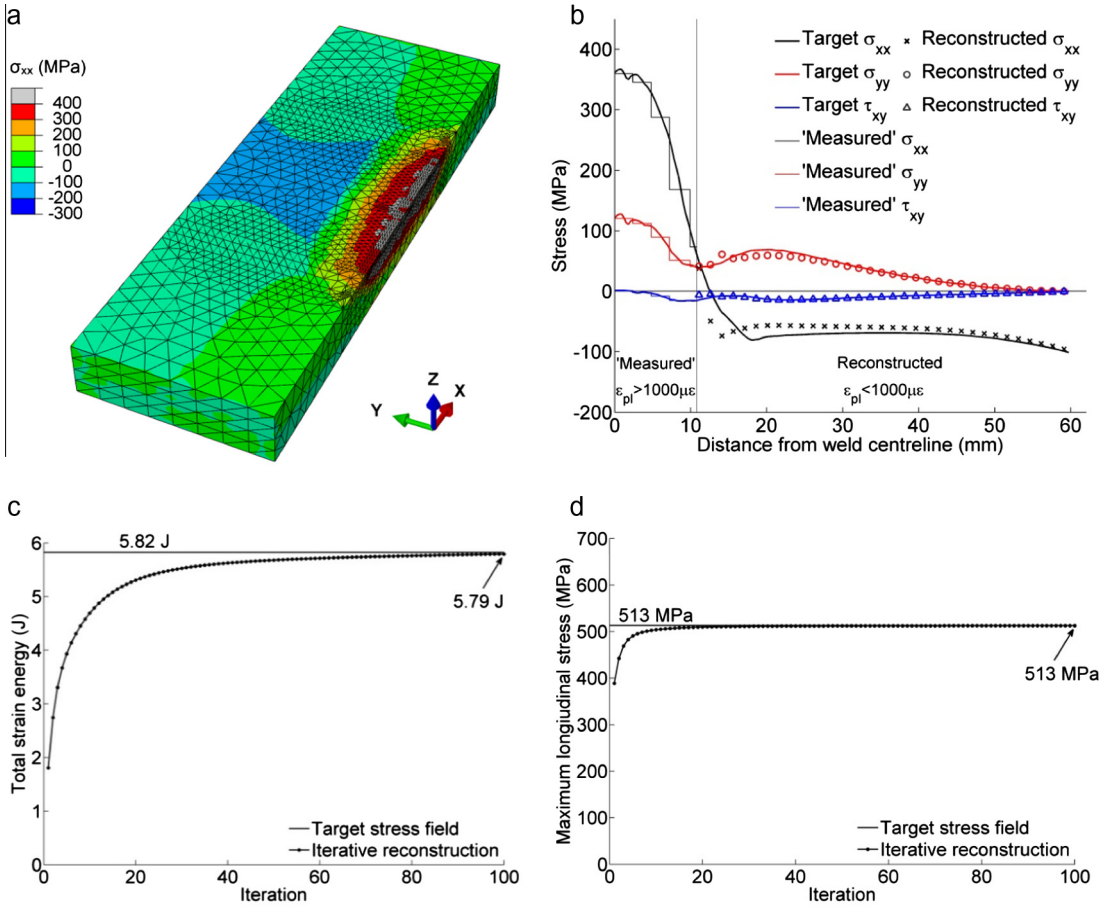

Fig. 11. Iterative method reconstruction from a data set with multiple forms of incompleteness and error: (a) Longitudinal stress (σ_{xx}), (b) comparison of stress components along the A–A line (see Fig. 2b), (c) iterative convergence of the total strain energy towards the target field, (d) convergence of the maximum longitudinal stress.

implicitly representing the incompatible forcing term in the compatibility equations (Eq. (2)). However, the method of accounting for this forcing term is different in each case: in the inverse eigenstrain method it is done by back-calculation of an eigenstrain distribution, in stress function methods it is done by selecting equilibrium-satisfying stress functions which characterise this incompatibility. In the present method is it done by ensuring that this incompatibility is represented within the measured stress data.

The assumptions required to implement the present technique are similar to those needed for the inverse eigenstrain method. Here, measurements must be made so that they include any regions containing eigenstrain, which results in a need for planning of any measurements so that they are appropriate for the reconstruction procedure. Similarly, in the inverse eigenstrain method it is necessary to use measurement locations which allow the eigenstrain distribution to be accurately characterised (Luckhoo et al., 2009). On the other hand, no assumptions regarding the dimensionality of the eigenstrain distribution and its tensor components are necessary for the present technique, whereas with the inverse eigenstrain method they would normally be required (Jun and Korsunsky, 2010; DeWald and Hill, 2006). Additionally, the method presented here is simpler to implement for complex three-dimensional stress states than either the inverse eigenstrain or stress function methods. The latter two rapidly become computationally demanding as the number of basis functions required to accurately represent the eigenstrain field increases. Consequently, although several examples exist of inverse eigenstrain and stress function methods being employed to reconstruct relatively complex states of stress (e.g. Kartal et al., 2012; Song and Korsunsky, 2011), reconstruction in the general three-dimensional case (classified by Jun & Korsunsky as a '3-3-3' problem type) has not yet been attempted using the inverse eigenstrain or stress function methods. Finally, the stress function and inverse eigenstrain methods involve the superposition of many stress solutions, requiring that the material is linearly elastic. The present method has no such requirement, and residual stress states in non-linear elastic materials can also be reconstructed.

6.4. Applications

This method of residual stress field reconstruction is most useful in cases where strain incompatibility is concentrated around a relatively small feature such as a weld. The method allows experimental measurements to be focused on such regions of interest while still providing insight into the nature of the complete stress field. This would be particularly useful in cases of structural integrity assessment where it is necessary to characterise both the residual stress state close to weld features in order to estimate fracture mechanics parameters, while at the same time having knowledge of the long-range components of the residual stress field. Such long-range residual stresses are commonly required for the purposes of estimating creep and stress-relaxation parameters such as elastic follow-up (Ainsworth, 1986).

It is emphasised that the method presented here is dependent upon being able to implicitly characterise the forcing term $\Xi(x,y,z)$ in Eq. (2), and is therefore strongly dependent on the completeness of the measured stress data (see Section 5). Therefore, just as with other methods its application to more complex stress

fields, such as the three-dimensional example given here, requires significantly more measurement data than for simpler cases.

7. Conclusions

- The complete stress field in a residually-stressed elastic body can be determined from the part of this stress field which exists in regions where the residual elastic strain is incompatible.
- Two methods of reconstructing the complete residual stress state from limited measurements using the finite element method have been introduced and applied to a modelled stress field in the NeT TG1 weld benchmark specimen. Of these two methods, the iterative implementation is recommended due to its better tolerance of incomplete measurement data.
- For exact reconstruction of the complete residual stress field, the part of stress field within the incompatible zone must be fully characterised. However, using synthetic measurement data with limited spatial resolution, limited spatial extent, a limited number of stress tensor components and limited accuracy, it has been shown that the proposed reconstruction method is relatively insensitive to these factors. This reconstruction method could therefore be used with incomplete and/or imprecise experimental residual stress data.

Acknowledgements

Funding for this research was provided under a joint Rolls-Royce/EDF Energy/Royal Academy of Engineering chair awarded to Prof. David Smith.

References

Abaqus Analysis User's Manual v6.12, 2012. Dassault Systèmes.
Achintha, M., Nowell, D., Shapiro, K., Withers, P.J., 2013. Eigenstrain modelling of residual stress generated by arrays of laser shock peening shots and determination of the complete stress field using limited strain measurements. Surf. Coat. Technol. 216, 68–77.
Ainsworth, R.A., 1986. The treatment of thermal and residual stresses in fracture assessments. Eng. Fract. Mech. 24, 65–76.
Bouchard, P.J., 2009. The NeT bead-on-plate benchmark for weld residual stress simulation. Int. J. Press. Vessels Pip. 86, 31–42.
Bouras, M., Boumaiza, A., Ji, V., Rouag, N., 2012. XRD peak broadening characterization of deformed microstructures and heterogeneous behavior of carbon steel. Theoret. Appl. Fract. Mech. 61, 51–56.
Daymond, M.R., Bourke, M.A.M., Dreele, R.B.V., Clausen, B., Lorentzen, T., 1997. Use of Rietveld refinement for elastic macrostrain determination and for evaluation of plastic strain history from diffraction spectra. J. Appl. Phys. 82, 1554–1562.
DeWald, A.T., Hill, M.R., 2006. Multi-axial contour method for mapping residual stresses in continuously processed bodies. Exp. Mech. 46, 473–490.
Do, S., Serasli, K., Smith, D.J., 2013. Combined measurement and finite element analysis to map residual stresses in welded components. In: Proceedings of the ASME 2013 Pressure Vessels and Piping Conference.
Eshelby, J.D., 1957. The determination of the elastic field of an ellipsoidal inclusion, and related problems. Proc. R. Soc., A 241, 376–396.
Faghidian, S.A., Goudar, D., Farrahi, G.H., Smith, D.J., 2012. Measurement, analysis and reconstruction of residual stresses. J. Strain Anal. Eng. Des. 47, 254–264.
Farrahi, G.H., Faghidian, S.A., Smith, D.J., 2009. Reconstruction of residual stresses in autofrettaged thick-walled tubes from limited measurements. Int. J. Press. Vessels Pip. 86, 777–784.
Farrahi, G.H., Faghidian, S.A., Smith, D.J., 2010. An inverse method for reconstruction of the residual stress field in welded plates. J. Pressure Vessel Technol., Trans. ASME 132, 612051–612059.
Ficquet, X., 2007. Development and Application of the Deep Hole Drilling Method. University of Bristol.
Hutchings, M.T., 1992. Neutron diffraction measurement of residual stress fields: overview and points for discussion. In: Measurement of Residual and Applied Stress Using Neutron Diffraction.
Jun, T.-S., Korsunsky, A.M., 2010. Evaluation of residual stresses and strains using the eigenstrain reconstruction method. Int. J. Solids Struct. 47, 1678–1686.
Jun, T.-S., Hofmann, F., Hofmann, M., Korsunsky, A.M., 2012. Residual stress characterization in 12%-Cr steel friction stir welds by neutron diffraction. J. Strain Anal. Eng. Des. 47, 203–213.
Kartal, M.E., Dunne, F.P.E., Wilkinson, A.J., 2012. Determination of the complete microscale residual stress tensor at a subsurface carbide particle in a single-crystal superalloy from free-surface EBSD. Acta Mater. 60, 5300–5310.
Korsunsky, A.M., 2009. Eigenstrain analysis of residual strains and stresses. J. Strain Anal. Eng. Des. 44, 29–43.
Korsunsky, A.M., Regino, G.M., 2007. Residual elastic strain in autofrettaged tubes: variational analysis by the eigenstrain finite element method. J. Appl. Mech., Trans. ASME 74, 717–722.
Krawitz, A.D., 2011. Neutron strain measurement. Mater. Sci. Technol. 27, 589–603.
Lei, Y., O'Dowd, N.P., Webster, G.A., 2000. Fracture mechanics analysis of a crack in a residual stress field. Int. J. Fract. 106, 195–216.
Luckhoo, H.T., Jun, T.-S., Korsunsky, A.M., 2009. Inverse eigenstrain analysis of residual stresses in friction stir welds. Procedia Eng. 1, 213–216.
Martins, R.V., Ohms, C., Decroos, K., 2010. Full 3D spatially resolved mapping of residual strain in a 316L austenitic stainless steel weld specimen. Mater. Sci. Eng., A 527, 4779–4787.
MATLAB®, version 4.14.0.739 (R2012a). The Mathworks Inc., Natick, USA.
Mura, T., 1987. Micromechanics of Defects in Solids. Kulwer Academic Publishers, Dortrecht, The Netherlands.
Smith, M.C., Smith, A.C., 2009. NeT bead-on-plate round robin: comparison of residual stress predictions and measurements. Int. J. Press. Vessels Pip. 86, 79–95.
Song, X., Korsunsky, A.M., 2011. Fully two-dimensional discrete inverse eigenstrain analysis of residual stresses in a railway rail head. J. Appl. Mech., Trans. ASME 78.
Timoshenko, S.P., Goodier, J.N., 1970. Theory of Elasticity, third ed. McGraw-Hill.
Wimpory, R.C., Ohms, C., Hofmann, M., Schneider, R., Youtsos, A.G., 2009a. Statistical analysis of residual stress determinations using neutron diffraction. Int. J. Press. Vessels Pip. 86, 48–62.
Wimpory, R.C., Ohms, C., Hofmann, M., Schneider, R., Youtsos, A.G., 2009b. Corrigendum to Statistical analysis of residual stress determinations using neutron diffraction. Int. J. Press. Vessels Pip. 86, 721.
Winholtz, R.A., Krawitz, A.D., 1996. The effect of assuming the principal directions in neutron diffraction measurement of stress tensors. Mater. Sci. Eng., A 205, 257–258.
Withers, P.J., 2007. Residual stress and its role in failure. Rep. Prog. Phys. 70, 2211–2264.
Withers, P.J., Bhadeshia, H.K.D.H., 2001. Residual stress: part 1 – measurement techniques. Mater. Sci. Technol. 17, 355–365.
Withers, P.J., Turski, M., Edwards, L., Bouchard, P.J., Buttle, D.J., 2008. Recent advances in residual stress measurement. Int. J. Press. Vessels Pip. 85, 118–127.